

ENGINEERING ANALYSIS INC AMES IA F/B 20/4
COMPUTATION OF THREE-DIMENSIONAL SUPERSONIC VISCOUS FLOWS IN IN--ETC(1)
MAR 80 J C TANNEHILL, D A ANDERSON F33615-79-C-3000

IN--ETC(U)

F33615-79-C-3000

ML

AFWAL-TR-80-3017

144

END
DATE
FILMED
8-80
DTIC

AFWAL-TR-80-3017

ADA 085857

COMPUTATION OF THREE-DIMENSIONAL SUPERSONIC VISCOUS FLOWS IN INTERNAL CORNERS

Engineering Analysis, Inc.
3621 Woodland St.
Ames, Iowa 50010

March 1980

TECHNICAL REPORT AFWAL-TR-80-3017

Final Report for Period 15 January 1979 - 15 January 1980

Approved for public release; distribution unlimited

FLIGHT DYNAMICS LABORATORY
AIR FORCE WRIGHT AERONAUTICAL LABORATORIES
AIR FORCE SYSTEMS COMMAND
WRIGHT-PATTERSON AIR FORCE BASE, OHIO 45433

RECEIVED
JUN 25 1980

A

DDC FILE COPY

392203

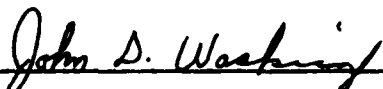
80 6 20 163

NOTICE

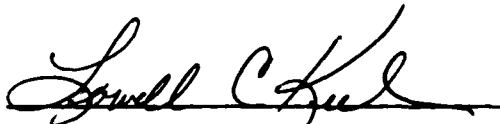
When Government drawings, specifications, or other data are used for any purpose other than in connection with a definitely related Government procurement operation, the United States Government thereby incurs no responsibility nor any obligation whatsoever; and the fact that the government may have formulated, furnished, or in any way supplied the said drawings, specifications, or other data, is not to be regarded by implication or otherwise as in any manner licensing the holder or any other person or corporation, or conveying any rights or permission to manufacture, use, or sell any patented invention that may in any way be related thereto.

This report has been reviewed by the Information Office (OI) and is releasable to the National Technical Information Service (NTIS). At NTIS, it will be available to the general public, including foreign nations.

This technical report has been reviewed and is approved for publication.




JOHN D. WASKIEWICZ, 1 LT, USAF
Project Engineer



LOWELL C. KEEL, MAJOR, USAF
Chief, Aerodynamics & Airframe Branch

FOR THE COMMANDER


PETER A. BUTKEWICZ, COLONEL, USAF
Chief, Aeromechanics Division

"If your address has changed, if you wish to be removed from our mailing list, or if the addressee is no longer employed by your organization please notify AFWAL/FIMM, W-PAFB, OH 45433 to help us maintain a current mailing list".

Copies of this report should not be returned unless return is required by security considerations, contractual obligations, or notice on a specific document.

SECURITY CLASSIFICATION OF THIS PAGE (When Data Entered)

REPORT DOCUMENTATION PAGE		READ INSTRUCTIONS BEFORE COMPLETING FORM
1. REPORT NUMBER (18) AFWAL-TR-80-3017	2. GOVT ACCESSION NO. AD-A085 857	3. RECIPIENT'S CATALOG NUMBER NPT
4. TITLE (and Subtitle) (6) COMPUTATION OF THREE-DIMENSIONAL SUPERSONIC VISCIOUS FLOWS IN INTERNAL CORNERS	5. TYPE OF REPORT & PERIOD COVERED (9) Final 15 Jan 79 - 15 Jan 80	6. PERFORMING ORG REPORT NUMBER
7. AUTHOR(s) (16) John C. Tannehill, Dale A. Anderson	8. CONTRACT OR GRANT NUMBER(s) (15) F33613-79-C-3000	
9. PERFORMING ORGANIZATION NAME AND ADDRESS Engineering Analysis, Inc. 3621 Woodland St. Ames, Iowa 50010	10. PROGRAM ELEMENT PROJECT AREA & WORK UNIT NUMBER 61102F (16) 2307N420	
11. CONTROLLING OFFICE NAME AND ADDRESS Flight Dynamics Laboratory (AFWL/FIMM) Air Force Wright Aeronautical Laboratories Wright-Patterson Air Force Base, Ohio 45433	12. REPORT DATE (11) Mar 1980	13. NUMBER OF PAGES (17) 53
14. MONITORING AGENCY NAME & ADDRESS (if different from Controlling Office) (13) 53	15. SECURITY CLASS. of this report Unclassified	15a. DECLASSIFICATION/DOWNGRADING SCHEDULE
16. DISTRIBUTION STATEMENT (of this Report) "Approved for Public Release" Distribution Unlimited		
17. DISTRIBUTION STATEMENT (of the abstract entered in Block 20, if different from Report)		
18. SUPPLEMENTARY NOTES		
19. KEY WORDS (Continue on reverse side if necessary and identify by block number) Axial Corner Flow Supersonic Viscous Flow Computational Fluid Dynamics		
20. ABSTRACT (Continue on reverse side if necessary and identify by block number) Three-dimensional, supersonic viscous flows in internal corners are computed by solving the unsteady Navier-Stokes equations subject to a local conical assumption. These governing equations are solved using MacCormack's explicit finite-difference scheme. A generalized coordinate system is employed which permits the grid to be refined near walls as well as in interaction regions so that viscous details can be properly resolved. Both shock fitting and shock capturing techniques are used. Two different corner flowfields are computed and the results are compared with experimental data and previous		

DD FORM 1 JAN 73 1473 EDITION OF 1 NOV 65 IS OBSOLETE

SECURITY CLASSIFICATION OF THIS PAGE (When Data Entered)

AD-A085 857

4/P

SECURITY CLASSIFICATION OF THIS PAGE(When Data Entered)

Block 20. Abstract (continued)

numerical solutions of the complete Navier-Stokes equations.

SECURITY CLASSIFICATION OF THIS PAGE(When Data Entered)

FOREWORD

This work was performed by Engineering Analysis, Inc., Ames, Iowa, from January 15, 1979 to January 15, 1980 under Air Force Contract F33615-79-C-3000. The authors wish to thank Lt. John D. Waskiewicz who served as Project Engineer for this study. The authors would also like to express their sincere gratitude to Dr. J. L. [redacted] and Dr. W. L. Hankey, Jr. for their helpful suggestions during the investigation.

A

TABLE OF CONTENTS

SECTION	PAGE
I INTRODUCTION	1
II GOVERNING EQUATIONS	6
III NUMERICAL SOLUTION OF EQUATIONS	11
1. Grid Generation	11
2. Finite Difference Scheme	15
3. Boundary Conditions	16
4. Initial Conditions	17
IV RESULTS	18
1. West and Korkegi Case	18
2. Cooper and Hankey Case	29
V CONCLUSIONS	41
REFERENCES	43

LIST OF ILLUSTRATIONS

FIGURE		PAGE
1	Axial Corner Flow	2
2	Computational Domains in Physical Plane	12
3	Computational Planes	14
4	Computational Mesh (shock fitting)	19
5	Density Contours (shock fitting)	21
6	Mach Number Contours (shock fitting)	22
7	Computational Mesh (shock capturing)	23
8	Density Contours (shock capturing)	25
9	Mach Number Contours (shock capturing)	26
10	Impact Pressure Distribution (shock capturing)	27
11	Comparison of Wall Pressures	28
12	Inviscid Details of Flowfield	30
13	Computational Mesh	31
14	Comparison of Impact Pressure Contours	33
15	Comparison of Impact Pressure Distributions ($0.09 < y/x < 0.4$)	34
16	Comparison of Impact Pressure Distributions ($0.00 < y/x < 0.09$)	35
17	Density Contours	36
18	Mach Number Contours	37
19	Total Temperature Contours	38
20	Comparison of Wall Pressures	39

LIST OF SYMBOLS

e	specific internal energy
e_t	total energy
j	mesh point location in ξ direction
k	mesh point location in η direction
L	dimensional length
M	Mach number
p	pressure
Pr	Prandtl number
q_x, q_y, q_z	components of heat flux vector
Re_L	Reynolds number
s	stretching function
t	time
T	temperature
u, v, w	velocity components in x, y, z directions
V	magnitude of velocity vector
V_1	fluid velocity normal to shock
x, y, z	Cartesian coordinates
$\bar{x}, \bar{y}, \bar{z}$	Cartesian coordinates on body surface
α, β, γ	conical coordinates
$\bar{\beta}$	stretching parameter
γ	specific heat ratio
δ	length of coordinate ray
δ_t	shock velocity
ζ, η	transformed coordinates

θ	angle of coordinate ray
μ	viscosity coefficient
ρ	density
$\sigma_{xx}, \sigma_{yy}, \sigma_{zz}$	normal stress components
$\tau_{xy}, \tau_{xz}, \tau_{yz}$	shearing stress components

Subscripts

b	body point
w	wall value
∞	freestream value
t	$\partial/\partial t$ or total condition
β	$\partial/\partial \beta$
γ	$\partial/\partial \gamma$
ζ	$\partial/\partial \zeta$
η	$\partial/\partial \eta$

SECTION I

INTRODUCTION

The flow field produced in the neighborhood of two intersecting surfaces in supersonic flow has been a subject of interest to design engineers for many years. These corner flows appear repeatedly in supersonic inlet systems, at wing-fuselage intersections and in conjunction with control surface deflections. The flow field near an axial corner is a strong interference flow which significantly influences the expected values of heat transfer and skin friction. For this reason, substantial effort has been expended in exploring the details of these axial corner flows.

The flow structure in a typical axial corner formed by supersonic flow over two intersecting compression surfaces is shown in Figure 1. The shock structure includes the shock waves produced by the intersecting wedges, the corner shock and the compression shock system which occurs when moving along the wedge surfaces into the corner. The triple points (where the corner shock, the wedge shocks and the embedded shock waves intersect) are joined to the corner by a viscous shear layer. The embedded shocks may produce separation in a plane normal to the direction of flow. The structure of corner flow was first detailed in the laminar case through the experiments of Charwat and Redekopp (Ref. 1) and by West and Korkegi (Ref. 2) for turbulent flow.

Numerous studies of the flow in an axial corner have been conducted using computational methods. Kutler (Ref. 3) and Shanker et al. (Ref. 4) have solved for the inviscid flow in an axial corner using the assumption

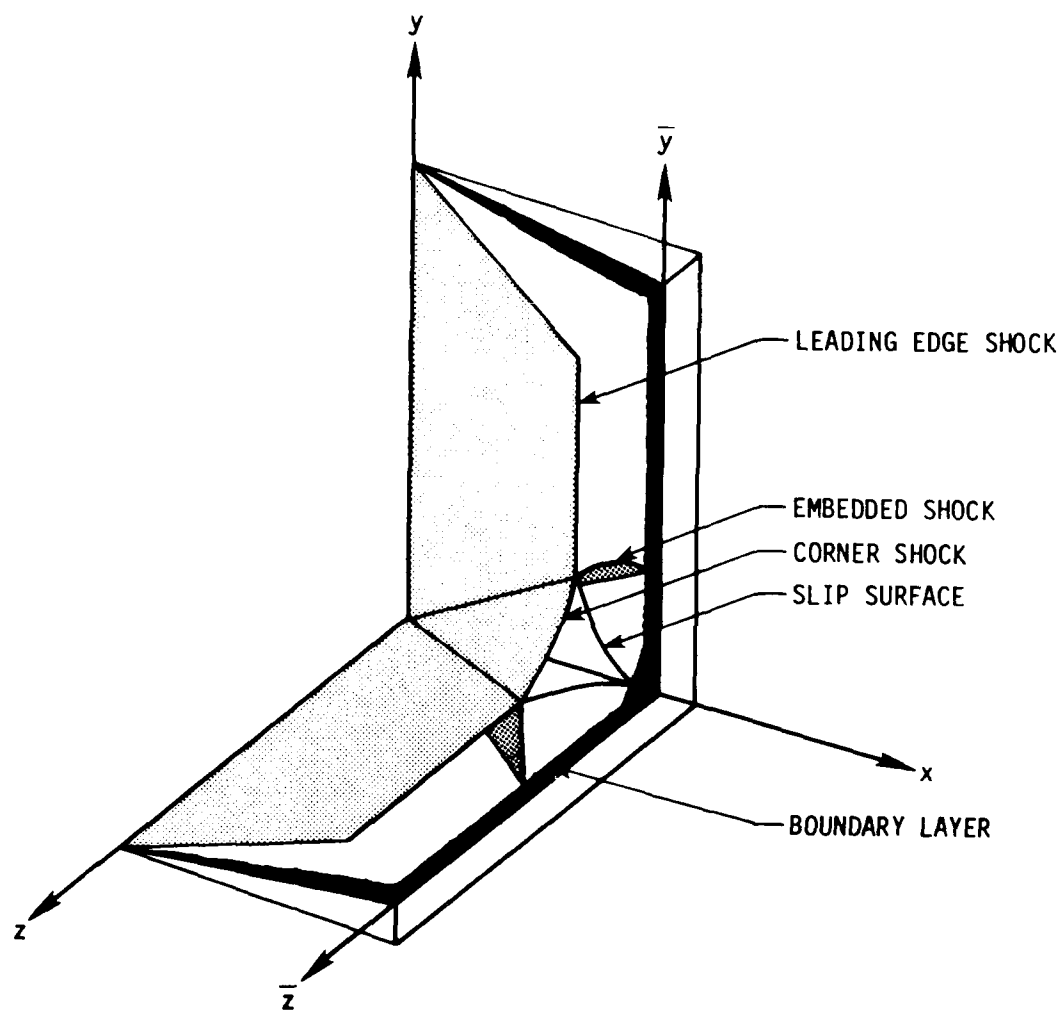


Figure 1. Axial Corner Flow

of conical symmetry. While these investigators used shock capturing, Marconi (Ref. 5) recently presented an inviscid solution to the corner flow problem using shock fitting. Results of these investigations showed accurate resolution of the shock wave and shear layer locations (for high Reynolds number experiments) although the peak pressure levels are sometimes underpredicted because viscous interaction effects are not included. An obvious disadvantage of these inviscid analyses is that they cannot predict heat transfer or skin friction. Cresi et al. (Ref. 6) and Rubin and Lin (Ref. 7) have studied the viscous flow in an axial corner near the leading edge. Their results are for a merged layer problem and are not valid at large distances from the leading edge. Faced with the limitations inherent in the merged layer and inviscid solutions, finite-difference methods were used to solve the full Navier-Stokes equations for supersonic flow in an axial corner. Shang and Hankey (Ref. 8) and Hung and MacCormack (Ref. 9) have obtained solutions for the laminar flow case while solutions for turbulent flow have been computed by Hung and MacCormack (Ref. 10) and Shang et al. (Ref. 11). While the results from the solutions of the Navier-Stokes equations agree well with experimental data, the usefulness of this approach is severely restricted by the large computer times required. Consequently, alternative methods of obtaining solutions for axial corner flows need to be developed.

The fully three-dimensional flow in the axial corner suggests that simplifying assumptions be made in order to reduce the required computational times to reasonable levels. In inviscid flows the conical flow assumption reduces a class of three-dimensional problems to an

essentially two-dimensional set. The conical flow assumption for inviscid flows makes use of the fact that a significant length scale is missing in the conical direction and the domain of interest is bounded by conical boundaries. This leads to the requirement that no variations in the radial direction can occur. This is a self-similar solution which is the same for all constant radius planes but scales linearly with the radius. The concept of conical flow is strictly valid only for inviscid flows. However, the viscous portions of the same flow fields, as observed in experiments, appear to be strongly dominated by the inviscid flow.

Anderson (Ref. 12) suggested that in those flows strongly dominated by the inviscid flow, a quick way of computing a solution (which would include an estimate of heat transfer and skin friction) would be to solve the Navier-Stokes equations in time on the unit sphere with all derivatives in the radial direction set equal to zero. This technique provides the proper shock structure but is not a viscous conical flow. The local Reynolds number is determined by the radial position where the solution is computed. Consequently, the solution is not self-similar in the sense of inviscid conical flow. The solution is scaled through the local Reynolds number which remains in the resulting set of equations.

This simplifying assumption has been used by McRae (Ref. 13) to compute the laminar flow over cones while Vigneron et al. (Ref. 14) and Bluford (Ref. 15) used the same approach to determine the laminar flow over a delta wing. McRae and Hussaini (Ref. 16) have solved

for the turbulent flow over a cone at angle of attack. In all cases the inviscid and viscous structure of the flow agrees quite well with available experimental data which indicates that the original expectations of this computational approach have been more than realized. As a consequence, an estimate of both the inviscid and viscous structure of the flows can be made without the long computer run times associated with the full Navier-Stokes equations.

In the present study, the axial corner flow problem is solved for the first time using the unsteady, Navier-Stokes equations subject to the local conical assumption. These equations are solved using an explicit time dependent approach. Both shock fitting and shock capturing techniques are used. The shock fitting technique is well suited for computing a compression corner flowfield (see Figure 1) since the wedge and corner shocks form one boundary of the computational region. This shock boundary is treated as a moving discontinuity across which the Rankine-Hugoniot equations are applied. All other internal shocks are automatically "captured" in the finite-difference solution. For cases where both surfaces of the corner are not compression surfaces, the shock fitting technique is not applicable and the shock capturing approach is used throughout the flowfield. The present method is used to compute two different supersonic internal corner flows and the results are compared with experiment.

SECTION II

GOVERNING EQUATIONS

The Navier-Stokes equations for an unsteady three-dimensional flow without body forces or external heat addition can be written in non-dimensional, conservation-law form for a Cartesian coordinate system as:

$$\frac{\partial U}{\partial t} + \frac{\partial E}{\partial x} + \frac{\partial F}{\partial y} + \frac{\partial G}{\partial z} = 0 \quad (1)$$

where

$$U = \begin{bmatrix} \rho \\ \rho u \\ \rho v \\ \rho w \\ \rho e_t \end{bmatrix} \quad e_t = e + \frac{u^2 + v^2 + w^2}{2}$$

$$E = \begin{bmatrix} \rho u \\ p + \rho u^2 - \sigma_{xx} \\ \rho uv - \tau_{xy} \\ \rho uw - \tau_{xz} \\ (\rho e_t + p)u - u\sigma_{xx} - v\tau_{xy} - w\tau_{xz} - q_x \end{bmatrix}$$

$$F = \begin{bmatrix} \rho v \\ \rho uv - \tau_{xy} \\ p + \rho v^2 - \sigma_{yy} \\ \rho vw - \tau_{yz} \\ (\rho e_t + p)v - u\tau_{xy} - v\sigma_{yy} - w\tau_{yz} - q_y \end{bmatrix}$$

$$G = \begin{bmatrix} \rho w \\ \rho uw - \tau_{xz} \\ \rho vw - \tau_{yz} \\ p + \rho w^2 - \tau_{zz} \\ (\rho e_t + p)w - u\tau_{xz} - v\tau_{yz} - w\tau_{zz} - q_z \end{bmatrix}$$

and

$$\sigma_{xx} = \frac{2\mu}{3Re_L} \left(2 \frac{\partial u}{\partial x} - \frac{\partial v}{\partial y} - \frac{\partial w}{\partial z} \right)$$

$$\sigma_{yy} = \frac{2\mu}{3Re_L} \left(2 \frac{\partial v}{\partial y} - \frac{\partial u}{\partial x} - \frac{\partial w}{\partial z} \right)$$

$$\sigma_{zz} = \frac{2\mu}{3Re_L} \left(2 \frac{\partial w}{\partial z} - \frac{\partial u}{\partial x} - \frac{\partial v}{\partial y} \right)$$

$$\tau_{xy} = \frac{\mu}{Re_L} \left(\frac{\partial u}{\partial y} + \frac{\partial v}{\partial x} \right)$$

$$\tau_{xz} = \frac{\mu}{Re_L} \left(\frac{\partial u}{\partial z} + \frac{\partial w}{\partial x} \right)$$

$$\tau_{yz} = \frac{\mu}{Re_L} \left(\frac{\partial v}{\partial z} + \frac{\partial w}{\partial y} \right)$$

$$q_x = \frac{\mu}{(\gamma - 1)M_\infty^2 Re_L Pr} \frac{\partial T}{\partial x}$$

$$q_y = \frac{\mu}{(\gamma - 1)M_\infty^2 Re_L Pr} \frac{\partial T}{\partial y}$$

$$q_z = \frac{\mu}{(\gamma - 1)M_\infty^2 Re_L Pr} \frac{\partial T}{\partial z}$$

The coefficient of thermal conductivity has been removed in the preceding equations by assuming a constant Prandtl number. In this study, the coefficient of viscosity μ is given by Sutherland's equation and the following perfect gas equations of state are used:

$$p = (\gamma - 1)\rho e$$

and

(2)

$$T = \gamma M_{\infty}^2 p / \rho$$

The equations have been nondimensionalized as follows (dimensional quantities are denoted by a wavy bar or a subscript ∞)

$$\begin{aligned} x &= \frac{\tilde{x}}{L} & y &= \frac{\tilde{y}}{L} & z &= \frac{\tilde{z}}{L} & t &= \frac{\tilde{t}}{L/V_{\infty}} \\ u &= \frac{\tilde{u}}{V_{\infty}} & v &= \frac{\tilde{v}}{V_{\infty}} & w &= \frac{\tilde{w}}{V_{\infty}} \\ \rho &= \frac{\tilde{\rho}}{\rho_{\infty}} & p &= \frac{\tilde{p}}{\rho_{\infty} V_{\infty}^2} & T &= \frac{\tilde{T}}{T_{\infty}} & e &= \frac{\tilde{e}}{V_{\infty}^2} \\ \mu &= \frac{\tilde{\mu}}{\mu_{\infty}} \end{aligned} \quad (3)$$

where L is the dimensional length defined by the Reynolds number

$$Re_L = \frac{\rho_{\infty} V_{\infty} L}{\mu_{\infty}} \quad (4)$$

The following conical transformation is introduced

$$\begin{aligned} \alpha &= x \\ \beta &= y/x \\ \gamma &= z/x \end{aligned} \quad (5)$$

and Eq. (1) becomes

$$\frac{\partial}{\partial t} (\alpha^2 U) + \frac{\partial}{\partial \alpha} (\alpha^2 E) + \frac{\partial}{\partial \beta} (\alpha F - \alpha E) + \frac{\partial}{\partial \gamma} (\alpha G - \alpha E) = 0$$

The assumption of local conical self-similarity requires that

$$\frac{\partial E}{\partial \alpha} = 0$$

and Eq. (6) reduces to

$$\frac{\partial U}{\partial t} + \frac{\partial}{\partial \beta} (-\beta E + F) + \frac{\partial}{\partial \gamma} (-\gamma E + G) + 2E = 0$$

on the surface $\alpha = 1$. The following generalized transformation is then applied

$$\eta = \eta(\beta, \gamma, t)$$

$$\zeta = \zeta(\beta, \gamma)$$

and the final forms of the governing equations become

$$\frac{\partial \bar{U}}{\partial t} + \frac{\partial \bar{F}}{\partial \zeta} + \frac{\partial \bar{G}}{\partial \eta} + \bar{H} = 0$$

where

$$\bar{U} = U/J$$

$$\bar{F} = -(\beta \zeta_\beta + \gamma \zeta_\gamma) E/J + \zeta_\beta F/J + \zeta_\gamma G/J$$

$$\bar{G} = \eta_t \bar{U} - (\beta \eta_\beta + \gamma \eta_\gamma) E/J + \eta_\beta F/J + \eta_\gamma G/J$$

$$\bar{H} = 2E/J$$

and J is the Jacobian of the transformation:

$$J = \frac{\partial(\eta, \zeta)}{\partial(\beta, \gamma)} = 1 / \frac{\partial(\beta, \gamma)}{\partial(\eta, \zeta)} \quad (12)$$

The partial derivatives which appear in the viscous terms of E, F and G are transformed with the aid of the expressions

$$\begin{aligned} \frac{\partial}{\partial x} &= -(\beta\eta_\beta + \gamma\eta_\gamma) \frac{\partial}{\partial \eta} - (\beta\zeta_\beta + \gamma\zeta_\gamma) \frac{\partial}{\partial \zeta} \\ \frac{\partial}{\partial y} &= \eta_\beta \frac{\partial}{\partial \eta} + \zeta_\beta \frac{\partial}{\partial \zeta} \\ \frac{\partial}{\partial z} &= \eta_\gamma \frac{\partial}{\partial \eta} + \zeta_\gamma \frac{\partial}{\partial \zeta} \end{aligned} \quad (13)$$

The governing equations are a mixed set of hyperbolic-parabolic equations which can be solved using a time-dependent technique.

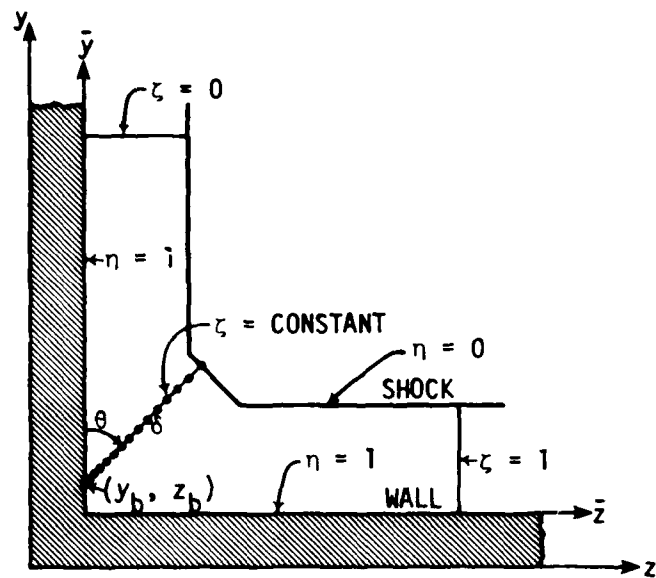
SECTION III

NUMERICAL SOLUTION OF EQUATIONS

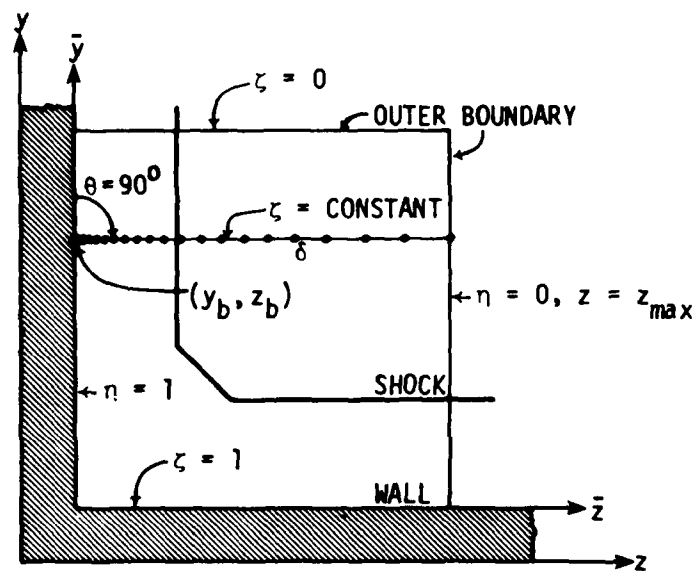
1. GRID GENERATION

The domain of computation on the surface $\alpha = 1$ is limited by the body and the outer shock for a shock-fitting calculation and is limited by the body and an outer boundary for the case of a shock-capturing calculation. These two types of computational domains are illustrated in Figure 2 for an axial corner formed by two intersecting wedges.

The computational grid is formed (Ref. 14) in a similar manner for both types of calculations. The $\zeta = \text{constant}$ lines are generated in the physical plane using straight rays which make an angle θ with the y axis and which emanate from the NJ grid points situated along the body surface. Along each ray (which has a length δ) NK grid points are positioned. The location of the grid points is arbitrary as long as they are regularly distributed. Normally they are clustered near the wall in order to properly resolve the boundary layer. For shock-fitting calculations, δ represents the shock standoff distance and is determined at each time step from the shock boundary condition. For shock-capturing calculations, δ remains fixed and is equal to $z_{\text{max}} - z_b$ for the case illustrated in Figure 2(b). The choice of the angle θ for each ray depends on the problem to be solved. For the shock-fitting configuration shown in Figure 2(a), θ varies between 90° and 0° , and for the shock-capturing configuration shown in Figure 2(b), θ equals 90° for all rays.



a) shock fitting



b) shock capturing

Figure 2. Computational Domains in Physical Plane

The computational planes (corresponding to the physical planes of Figure 2) are shown in Figure 3. The grid in the computational plane has the shape of a unit square with uniform spacing in each direction given by

$$\Delta\eta = \frac{1}{NK - 1} \quad \Delta\zeta = \frac{1}{NJ - 1} \quad (14)$$

so that $\eta = (k - 1)\Delta\eta$ and $\zeta = (j - 1)\Delta\zeta$.

For the calculations in this study, the physical and computational planes are related by the relations

$$\begin{aligned} y(j, k) &= y_b(j) + s(j, k) \cos [\theta(j)] \\ z(j, k) &= z_b(j) + s(j, k) \sin [\theta(j)] \end{aligned} \quad (15)$$

where $s(j, k)$ is the stretching function

$$s(j, k) = \delta \left\{ 1 - \bar{\beta} \left[\left(\frac{\bar{\beta} + 1}{\bar{\beta} - 1} \right)^\eta - 1 \right] / \left[1 + \left(\frac{\bar{\beta} + 1}{\bar{\beta} - 1} \right)^\eta \right] \right\} \quad (16)$$

which clusters more grid points near the wall ($\eta = 1$) as the stretching parameter $\bar{\beta}$ approaches one. The body grid points (y_b, z_b) can be clustered using the same type of stretching function. For example, in the shock-capturing configuration of Figure 2(b) the $\zeta = \text{constant}$ grid lines must be clustered near the $\zeta = 1$ wall in order to properly resolve the boundary layer.

The metrics η_β , η_γ , ζ_β and ζ_γ which appear in Eqs. (11) and (13) are evaluated using the relations

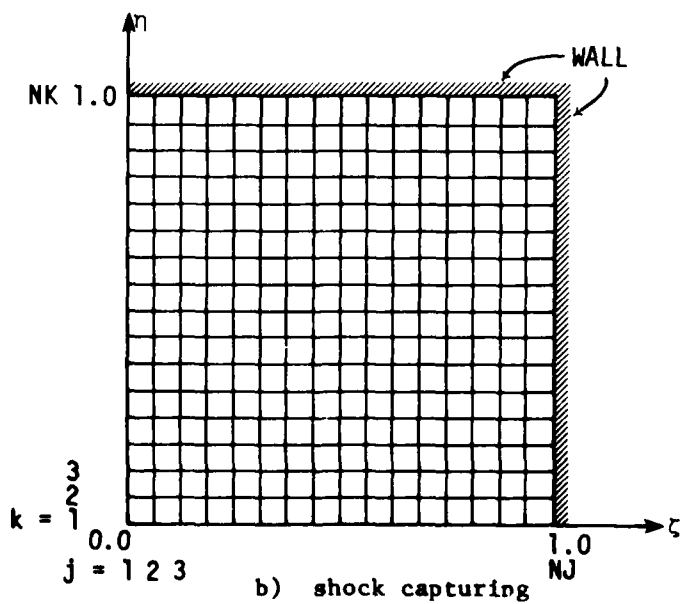
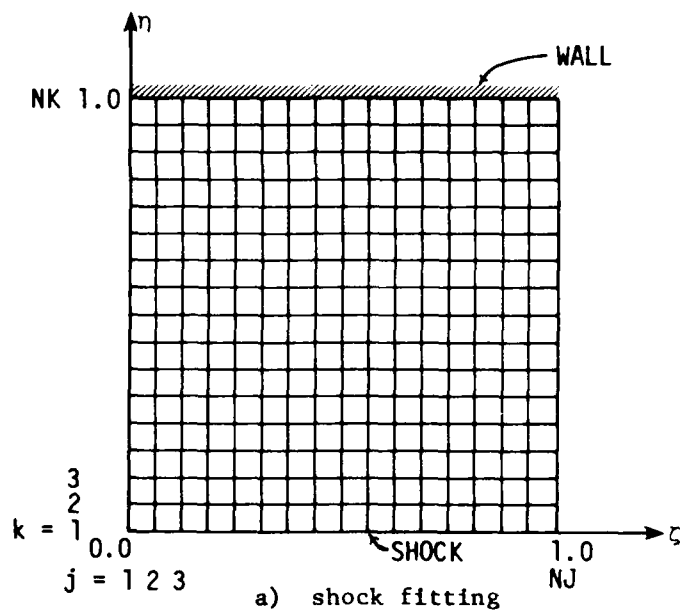


Figure 3. Computational Planes

$$\begin{aligned}
\eta_{\beta} &= J\gamma_{\beta} & \gamma_{\beta} &= -J\gamma_{\eta} \\
\eta_{\gamma} &= -J\beta_{\gamma} & \beta_{\gamma} &= J\beta_{\eta} \\
J &= 1/(\beta_{\eta}\gamma_{\gamma} - \beta_{\gamma}\gamma_{\eta})
\end{aligned} \tag{17}$$

where the derivatives β_{η} , β_{γ} , γ_{η} and γ_{γ} are computed numerically with central differences in the regularly spaced computational plane (Ref. 14). The metric coefficient η_t is obtained from the differentiation of the stretching function and is given by

$$\eta_t = 2\bar{\beta}s\delta_t / \left\{ [\bar{\beta}^2\delta^2 - (\delta - s)^2] \ln \left(\frac{\bar{\beta} + 1}{\bar{\beta} - 1} \right) \right\} \tag{18}$$

where δ_t is the shock velocity described later.

2. FINITE DIFFERENCE SCHEME

The standard, unsplit, MacCormack finite-difference scheme (Ref. 17) is used to solve the governing equations at each interior grid point. This explicit scheme has second-order accuracy in both space and time. When this algorithm is applied to Eq. (10), the following predictor-corrector equations result:

$$\begin{aligned}
\bar{u}_{j,k}^{n+1} &= \bar{u}_{j,k}^n - \frac{\Delta t}{\Delta \zeta} \left(\bar{F}_{j+1,k}^n - \bar{F}_{j,k}^n \right) - \frac{\Delta t}{\Delta \eta} \left(\bar{G}_{j,k+1}^n - \bar{G}_{j,k}^n \right) - \Delta t \bar{H}_{j,k}^n \\
\bar{u}_{j,k}^{n+1} &= 1/2 \left[\bar{u}_{j,k}^n + \bar{u}_{j,k}^{n+1} - \frac{\Delta t}{\Delta \zeta} \left(\bar{F}_{j,k}^{n+1} - \bar{F}_{j-1,k}^{n+1} \right) - \frac{\Delta t}{\Delta \eta} \left(\bar{G}_{j,k}^{n+1} - \bar{G}_{j,k-1}^{n+1} \right) \right. \\
&\quad \left. - \Delta t \bar{H}_{j,k}^{n+1} \right]
\end{aligned} \tag{19}$$

Using this finite-difference scheme, the computation is advanced in time from the initial conditions until the steady-state solution is reached. The allowable time step is computed using the empirical formula of Ref. 18 which modifies the inviscid CFL condition to approximately account for viscous effects. The fourth-order damping scheme introduced by MacCormack and Baldwin (Ref. 17) is used to suppress nonlinear instabilities.

3. BOUNDARY CONDITIONS

The flow conditions behind the shock boundary (for a shock-fitting calculation) are determined using a procedure similar to the one described in Ref. 18. At the beginning of the predictor step, the shock standoff distances are computed using

$$\overline{\delta^{n+1}} = \delta^n + \Delta t \delta_t^n \quad (20)$$

where the shock velocity δ_t is given by

$$\delta_t = \left\{ V_1 \left[(\beta \gamma_\zeta - \gamma \beta_\zeta)^2 + \beta_\zeta^2 + \gamma_\zeta^2 \right]^{1/2} - u_\infty (\beta \gamma_\zeta - \gamma \beta_\zeta) + v_\infty \gamma_\zeta - w_\infty \beta_\zeta \right\} / (\gamma_\zeta \cos \theta - \beta_\zeta \sin \theta) \quad (21)$$

and V_1 is the component of the fluid velocity normal to and measured with respect to the moving shock. The flow variables behind the shock, as well as V_1 , can be readily determined using Rankine-Hugoniot relations (Ref. 19) once the pressures behind the shock are known. These pressures are calculated using the standard MacCormack predictor equation at each grid point behind the shock. The corrector step is

similar to the predictor step except that the shock standoff distances are evaluated using the modified Euler corrector

$$\delta^{n+1} = \delta^n + \Delta t \left(\delta_t^n + \overline{\delta_t^{n+1}} \right) / 2 \quad (22)$$

and the pressures behind the shock are computed using a modified MacCormack corrector scheme in which the usual backward difference for $\partial \bar{G} / \partial n$ is replaced by a forward difference. The flow variables along the outer boundaries, $\zeta = 0$ and $\zeta = 1$ in Figure 2(a) and $\zeta = 0$ and $\eta = 0$ in Figure 2(b), are determined by assuming flow gradients parallel to the wall surfaces are zero. An exception to this occurs along the outer boundaries in the vicinity of the corner ($\zeta = 0, \eta = 0$) in Figure 2(b) where freestream conditions can be maintained. Along the wall boundaries, the velocities are set equal to zero and the temperature is specified for an isothermal wall. The pressure is determined by assuming the normal pressure gradient to be zero and the density is then calculated using the equation of state.

4. INITIAL CONDITIONS

The initial conditions for a shock fitting calculation are obtained by patching together inviscid wedge flow solutions. The initial conditions for a shock-capturing calculation are obtained by specifying freestream flow conditions at each grid point.

SECTION IV

RESULTS

1. WEST AND KORKEGI CASE

The present method has been used to compute a supersonic internal corner flowfield corresponding to a laminar experiment of West and Korkegi (Ref. 2). The corner is formed by the intersection of two wedges with identical wedge angles of 9.48° . The flow conditions are

$$\begin{array}{ll} M_\infty = 3.0 & T_\infty = 105^\circ\text{K} \\ Re_L = 0.39 \times 10^6 & T_w = 294^\circ\text{K} \\ Pr = 0.72 & \gamma = 1.4 \end{array}$$

The flowfield was computed using both the shock fitting and shock capturing approaches. In the shock fitting calculation, a mesh consisting of 31 grid points in the η direction and 50 grid points in the ζ direction was used and is shown in Figure 4 for the converged solution. Since the present corner configuration is symmetric the mesh could have been reduced to 31×25 , however, the entire corner region was computed here in order to serve as a check for future nonsymmetrical calculations. The mesh was refined near the walls using a stretching parameter $\bar{\beta}$ equal to 1.04. The body grid points were clustered near the axis of symmetry ($\zeta = 1/2$) using a similar type of stretching function with a stretching parameter equal to 1.12. The θ angles required for the $\zeta = \text{constant}$ grid lines were obtained by letting these straight rays be the radii of a circle.

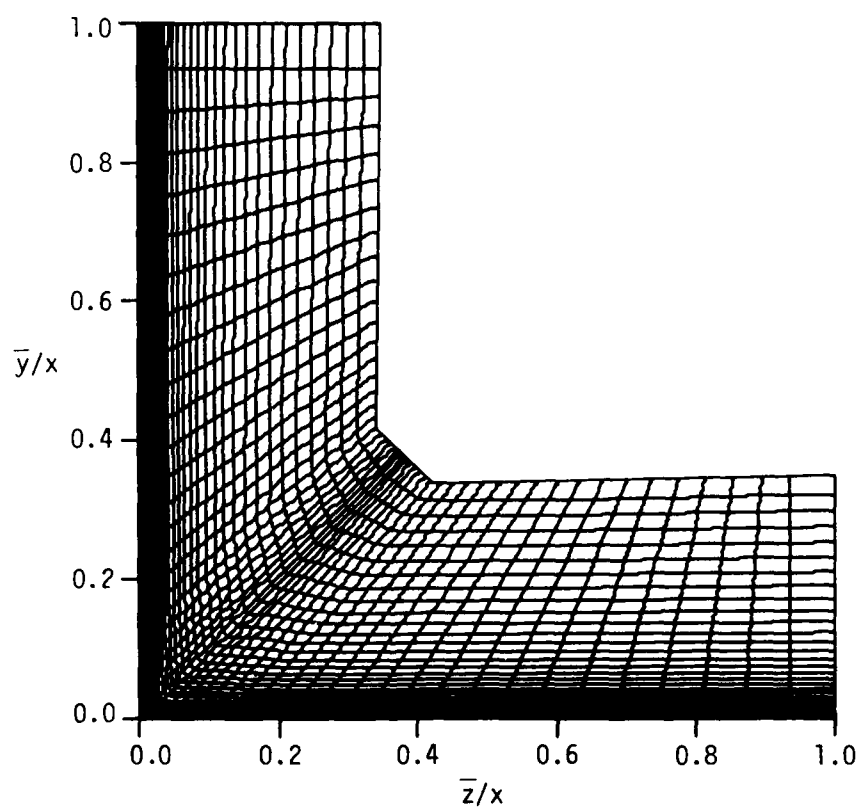


Figure 4. Computational Mesh (shock fitting)

The shock fitting calculation required about 5000 steps to converge. It was necessary to reverse the finite differencing in the ζ direction in the region $0 \leq \zeta \leq 1/2$ in order to eliminate a long period instability which appeared in the calculation. This instability is believed to be due to the stagnation point located at $\zeta = 1/2$. Previous investigators (Refs. 17 and 18) encountered a similar instability in the vicinity of an interior stagnation point. This instability is caused by the inability of the finite-difference scheme to readily distinguish a change in velocity direction when conservative variables are employed. The shock capturing calculation does not encounter this instability because the stagnation point is located at a corner of the computational domain.

The results of the shock fitting calculation are shown in Figures 5, 6, and 11. The flow structure in terms of density contours is shown in Figure 5. The embedded shocks and boundary layers are clearly visible in this contour plot. The locations of the shock waves and slip surfaces are in excellent agreement with the experiment. The thickening of the boundary layer outward from the embedded shock is due to flow separation. This separated flow region is less extensive than the region computed by Shang et al. (Ref. 11) using the complete Navier-Stokes equations. The Mach number contours are shown in Figure 6. These contours were drawn in increments (ΔM) of 0.1 starting at $M = 0$.

The shock capturing calculation utilized a fixed mesh consisting of 31×31 grid points and is shown in Figure 7. The mesh was refined equally near both walls using a stretching parameter $\bar{\beta}$ equal to 1.01.

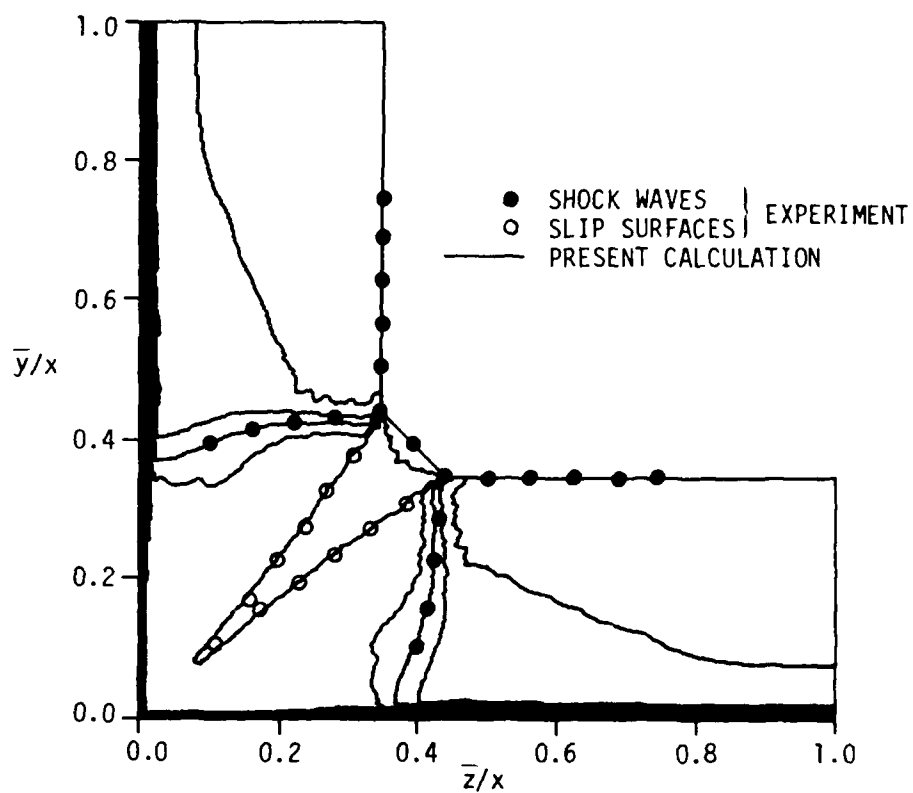


Figure 5. Density Contours (shock fitting)

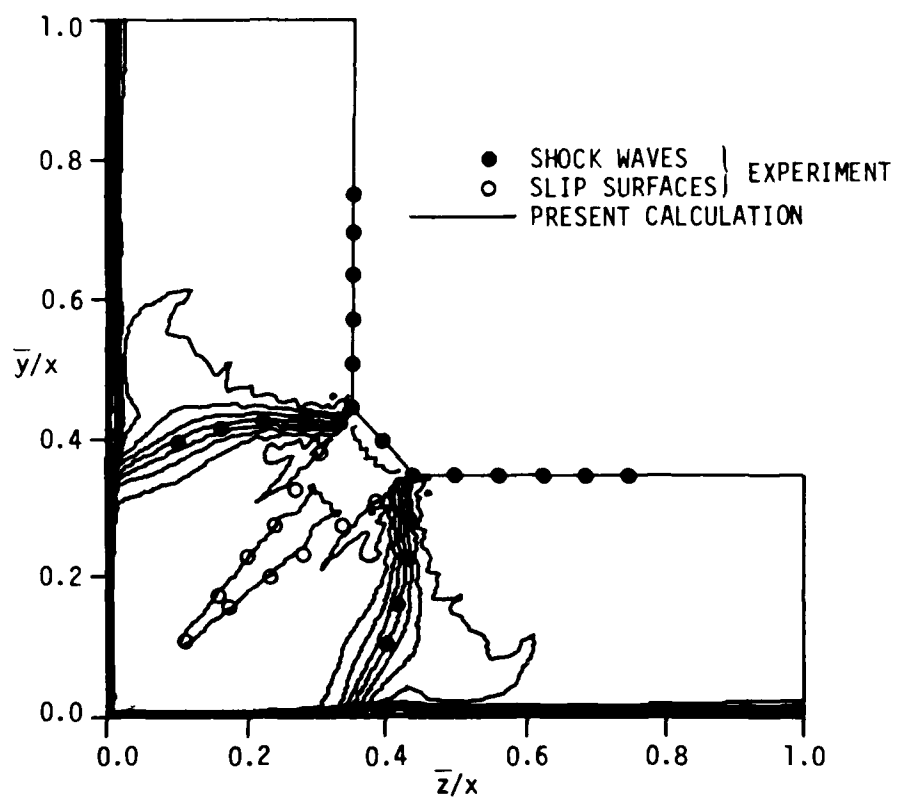


Figure 6. Mach Number Contours (shock fitting)

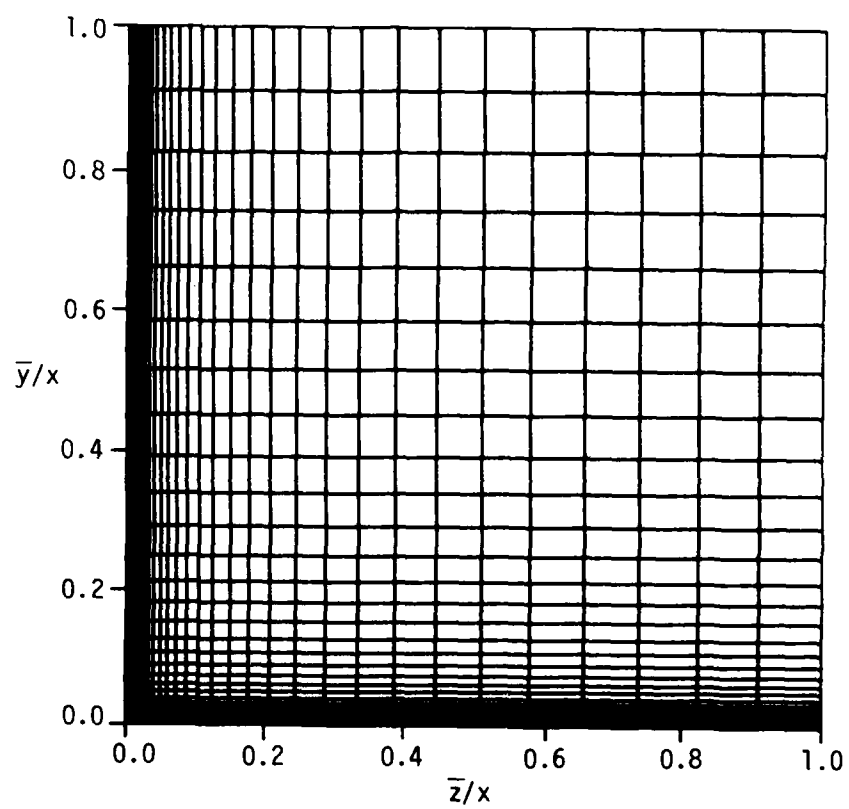


Figure 7. Computational Mesh (shock capturing)

This calculation also required about 5000 steps to converge to a steady state. The density and Mach number contour plots for this calculation are shown in Figures 8 and 9, respectively. These contour plots were drawn with the same increments in density and Mach number as the previous contour plots, Figures 5 and 6. The advantage of using the shock fitting procedure (whenever possible) is dramatically illustrated by comparing the contour plots for each type of calculation. The shock fitting solution exhibits a much "sharper" resolution of the flowfield details. The impact pressures (normalized by the stagnation pressure) are shown at various heights above one wedge surface in Figure 10. The rise in the impact pressure (except for $\bar{y}/x = 0.581$) on the right-hand side of the distribution is due to the imbedded shock wave. The impact pressure rise in the $\bar{y}/x = 0.581$ distribution is the result of the shock wave from the other wedge surface. The depressions in the impact pressure distributions are due to the slip surfaces which merge together near $\bar{y}/x = 0.08$.

The computed wall pressures for both the shock fitting and shock capturing calculations are compared in Figure 11 with the experimental data (Ref. 2) and the complete Navier-Stokes calculation of Shang et al. (Ref. 11). As would be expected, the present wall pressure results do not compare as well with the experiment as do the results from the complete Navier-Stokes calculation. The computed pressure rise in the separated flow region is less than that observed in the experiment. However, the present method does give a good engineering approximation to the wall pressure distribution at a fraction of the cost of a complete Navier-Stokes calculation. The present shock capturing calculation

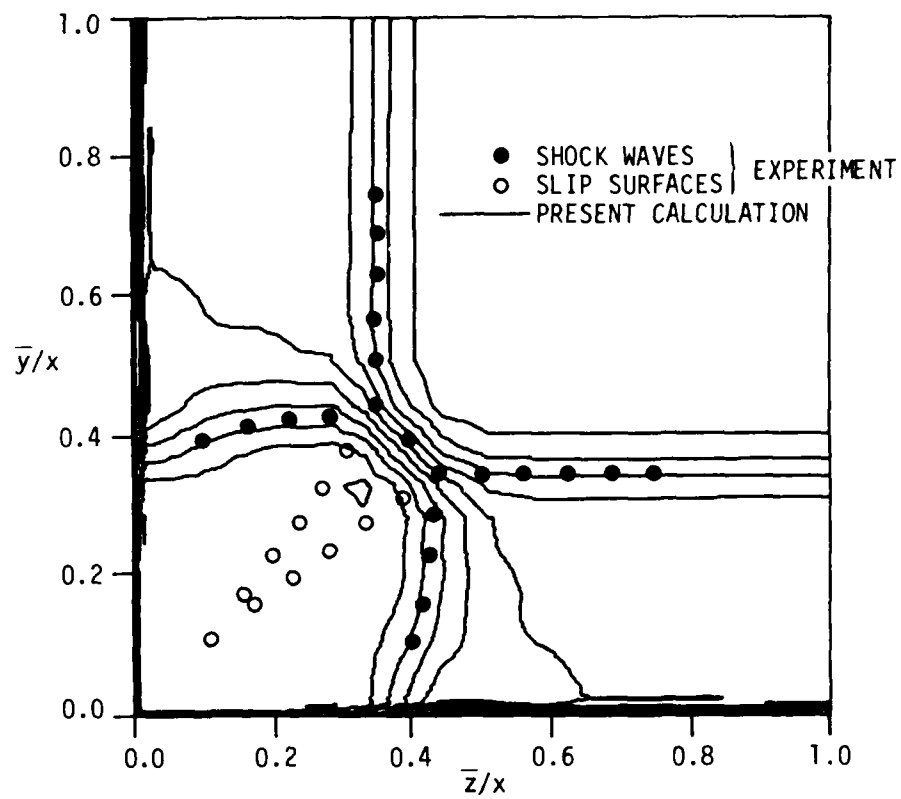


Figure 8. Density Contours (shock capturing)

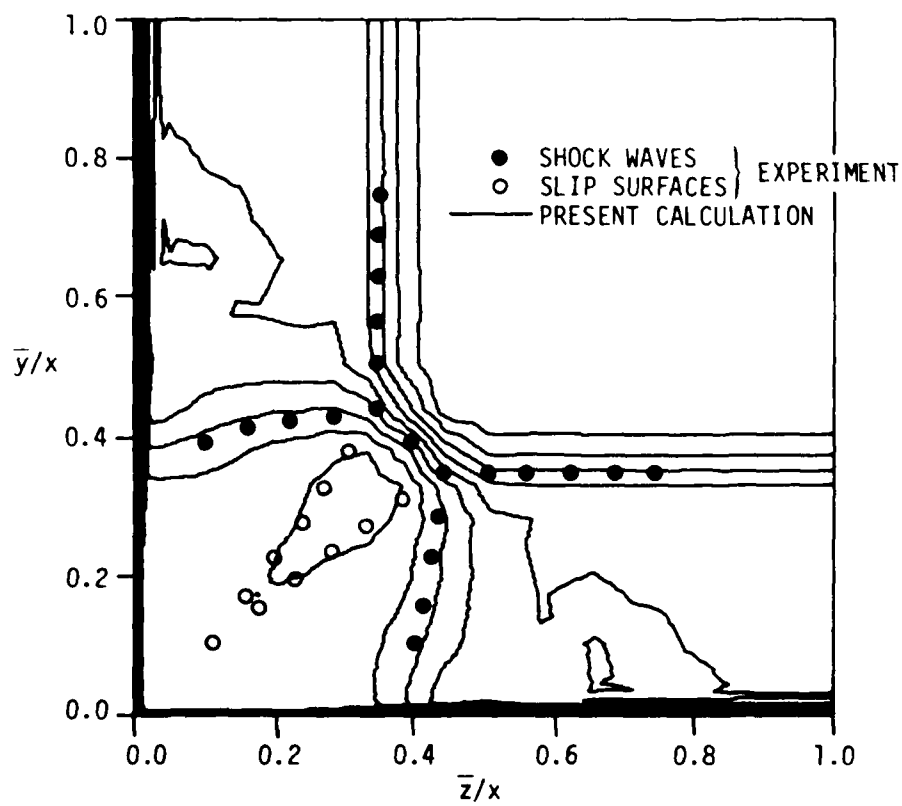


Figure 9. Mach Number Contours (shock capturing)

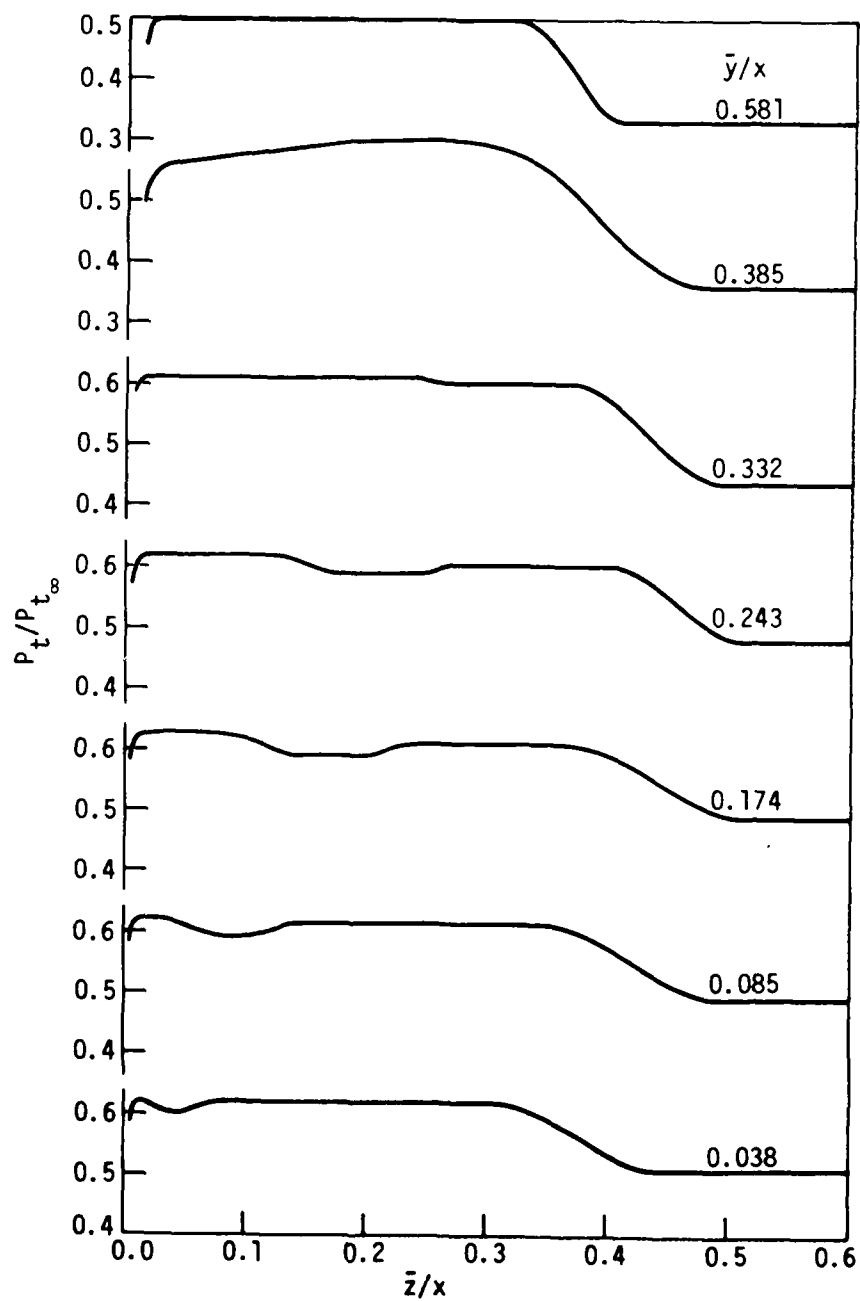


Figure 10. Impact Pressure Distribution (shock capturing)

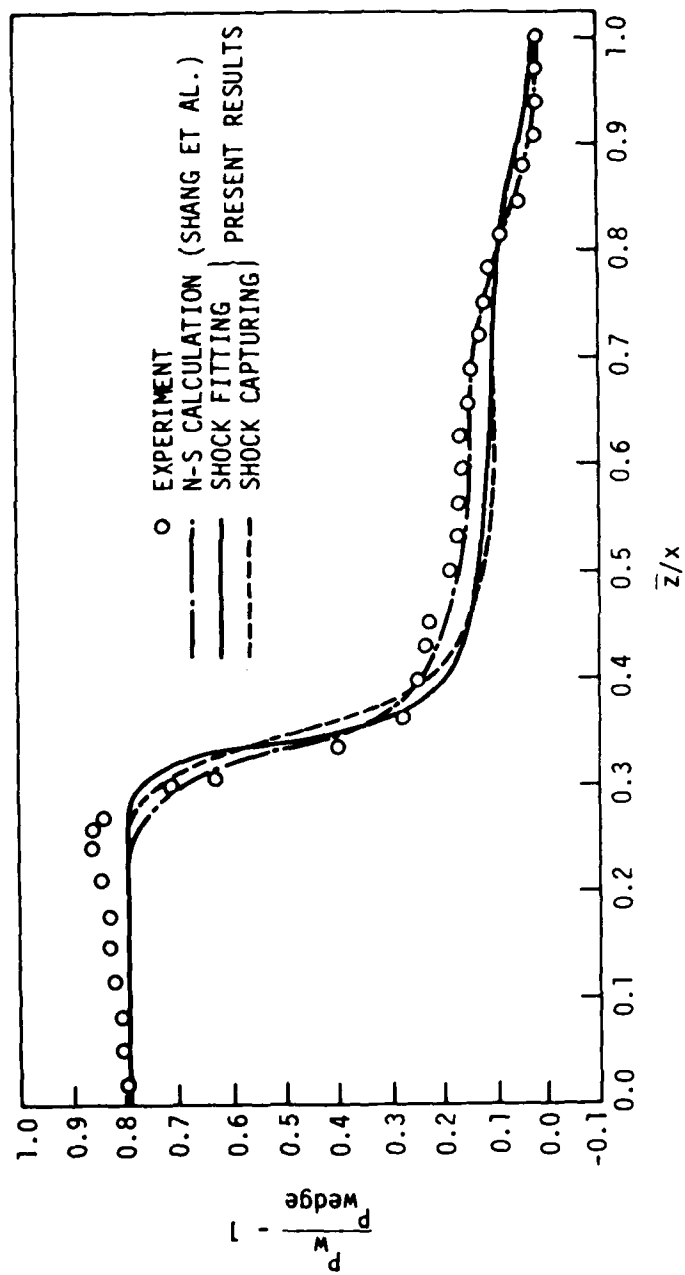


Figure 11. Comparison of Wall Pressures

required about 23 minutes of computer time on a CDC 7600 computer while the shock fitting calculation required about 43 minutes. The latter time could have been cut in half if the 31×25 mesh had been used instead of the 31×50 mesh. The shock fitting technique requires 16% more computer time (per grid point per time step) than does the shock capturing approach.

2. COOPER AND HANKEY CASE

The present method has been used to compute an unsymmetrical internal corner flowfield corresponding to a laminar experiment of Cooper and Hankey (Ref. 20). The inviscid details of this corner configuration are shown in Figure 12. This particular configuration offers a severe test for the present method since the flowfield is not conical. The actual flowfield depends crucially on the proper interaction of the flat plate boundary layer (and its induced shock) with the wedge shock. The flow conditions of this test case are

$$\begin{array}{ll} M_{\infty} = 12.5 & T_{\infty} = 367^{\circ}\text{K} \\ \text{Re}_L = 1.21 \times 10^6 & T_w = 31^{\circ}\text{K} \\ \text{Pr} = 0.72 & \gamma = 1.4 \end{array}$$

with a wedge angle of 15° . The flowfield was computed using the shock capturing approach since the shock fitting approach is not applicable. A mesh consisting of 31×31 grid points was used and is shown in Figure 13. The mesh was refined near both walls using a stretching parameter $\bar{\beta}$ equal to 1.01.

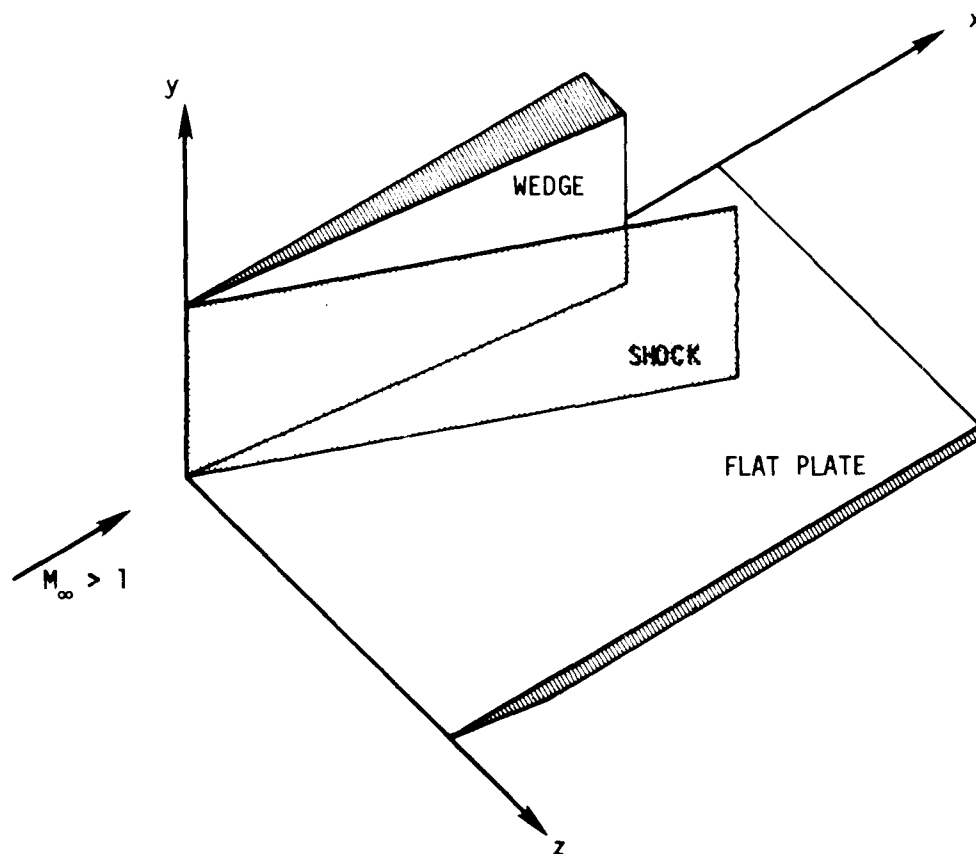


Figure 12. Inviscid Details of Flowfield

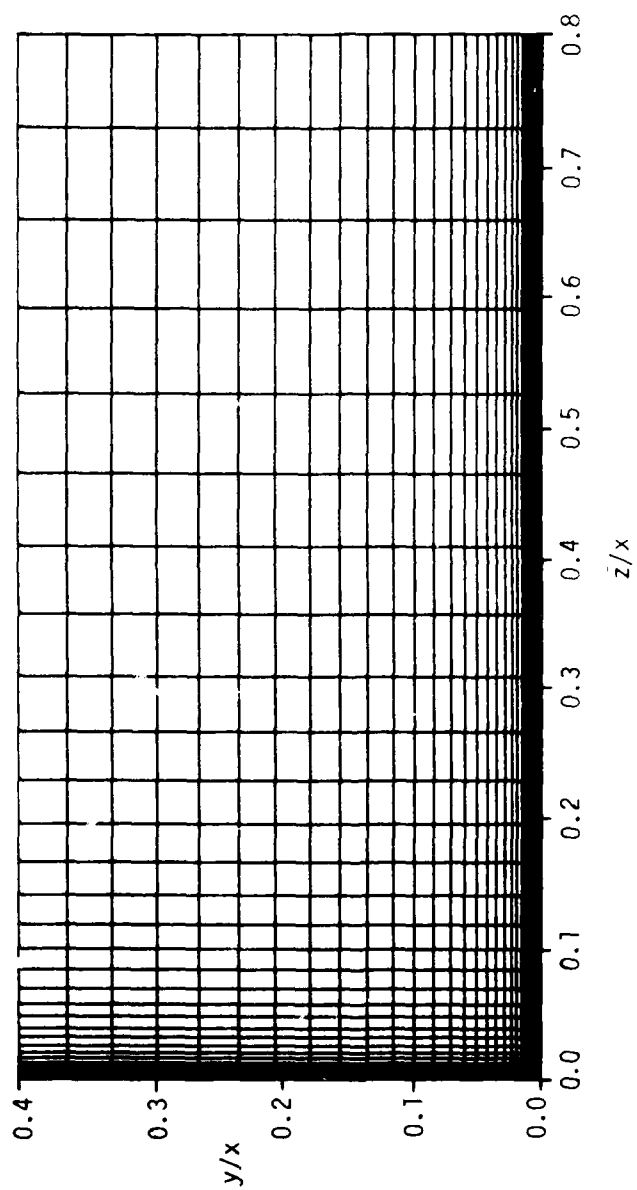
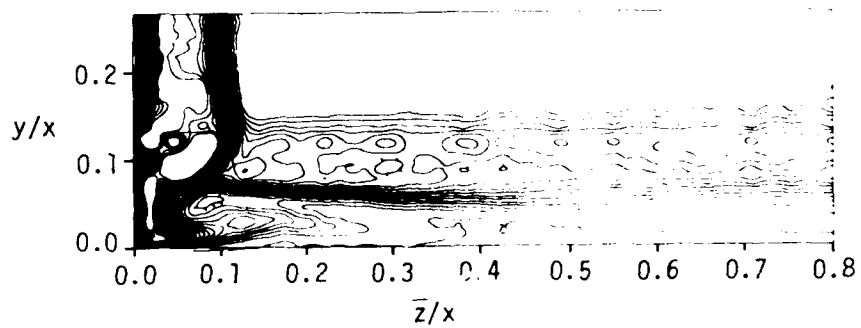


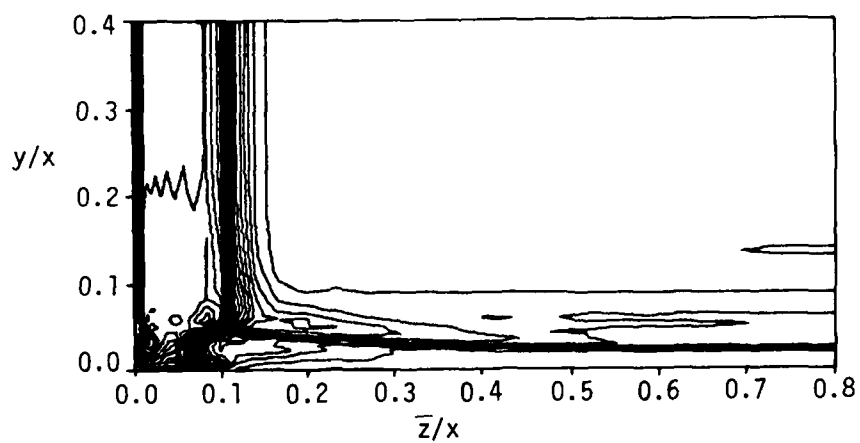
Figure 13. Computational Mesh

The calculation required about 4000 steps to converge to a steady state. The results of this calculation are shown in Figures 14-20. In Figure 14, a contour plot of the computed impact pressures is compared with the corresponding contour plot (same Δp_t) from the Navier-Stokes calculations of Shang and Hankey (Ref. 8). The contour plot of impact pressures from the present calculation compares qualitatively with the contour plot from the Navier-Stokes calculation. However, it is obvious that the present analysis does not properly compute the boundary layer thickness on the flat plate and consequently, the induced shock is not correctly located. In fact, the computed boundary layer thickness and the shock standoff distance are about half the values obtained in the Navier-Stokes calculation. As a result, the details of the computed interaction flowfield are compressed downward as seen in Figures 15 and 16. These figures compare the impact pressure distributions at various heights above the flat plate. For a given height, the present distribution compares reasonably well with the Navier-Stokes distribution at twice that height. This suggests that the present method could be used to obtain reasonable results for the given problem if an appropriate Reynolds number were chosen that gave the correct boundary layer thickness.

Contour plots for the computed densities, Mach numbers, and total temperatures are shown in Figures 17, 18 and 19. The increments used for these contour plots are $\Delta \rho = 0.25$, $\Delta M = 0.1$, and $\Delta \tilde{T}_t = 100^\circ \text{K}$. A comparison of the wall pressures is shown in Figure 20. Once again, the present method gives a good engineering approximation to the wall pressure distribution. As expected, the heat transfer results are



a) N-S calculation (Shang and Hankey)



b) Present calculation

Figure 14. Comparison of Impact Pressure Contours

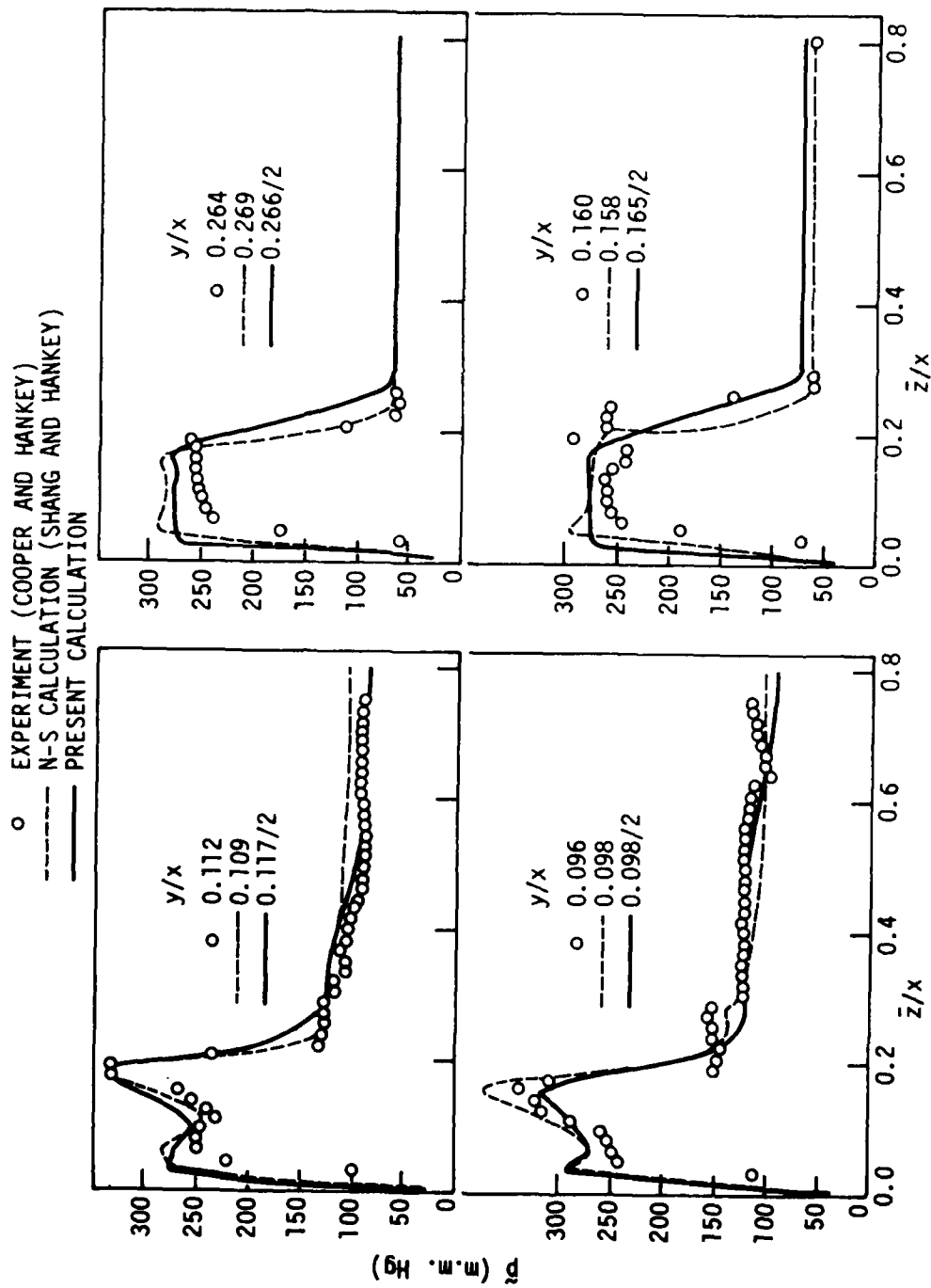


Figure 15. Comparison of Impact Pressure Distributions ($0.09 < y/x < 0.4$)

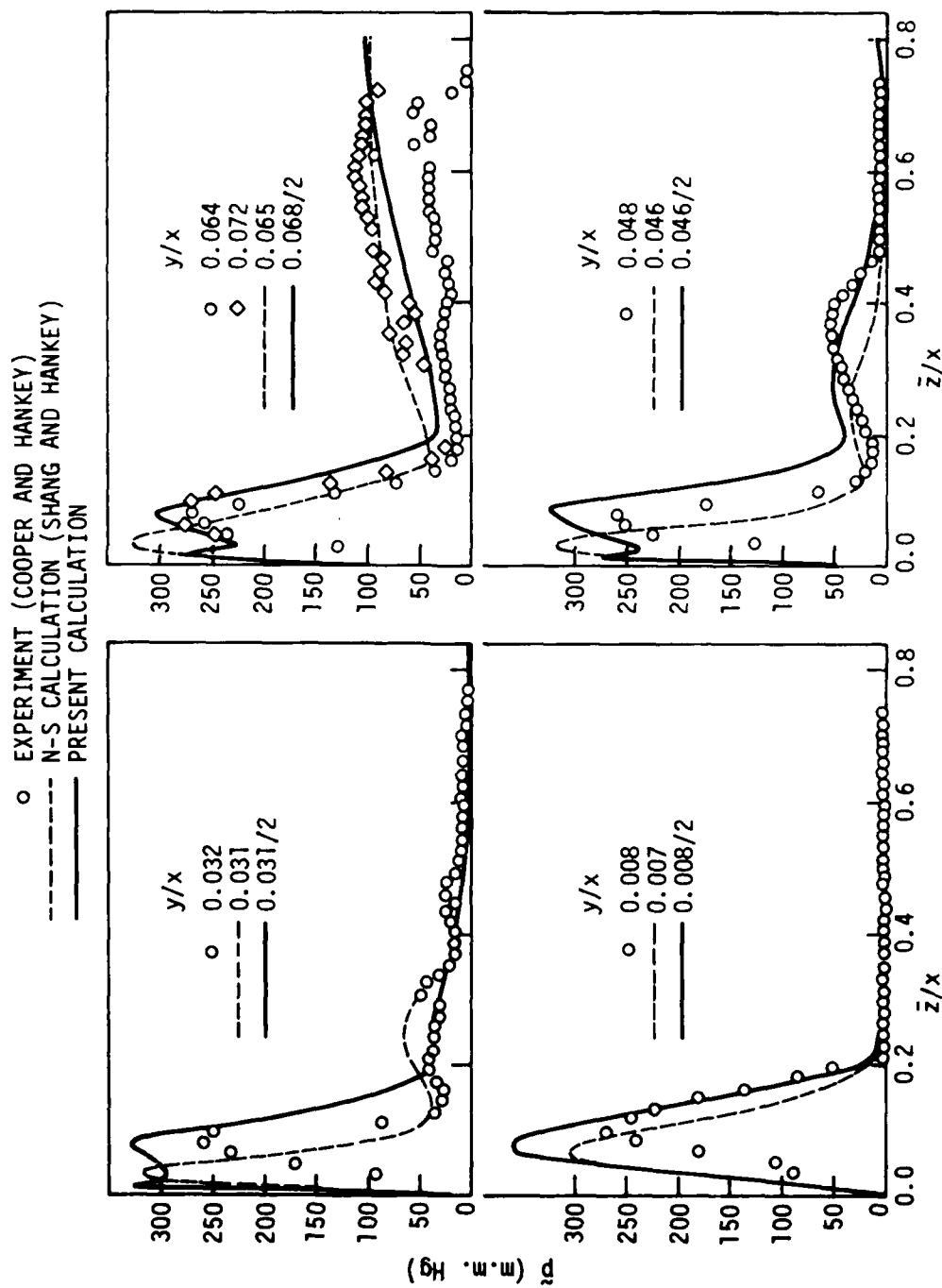


Figure 16. Comparison of Impact Pressure Distributions ($0.00 < y/x < 0.09$)

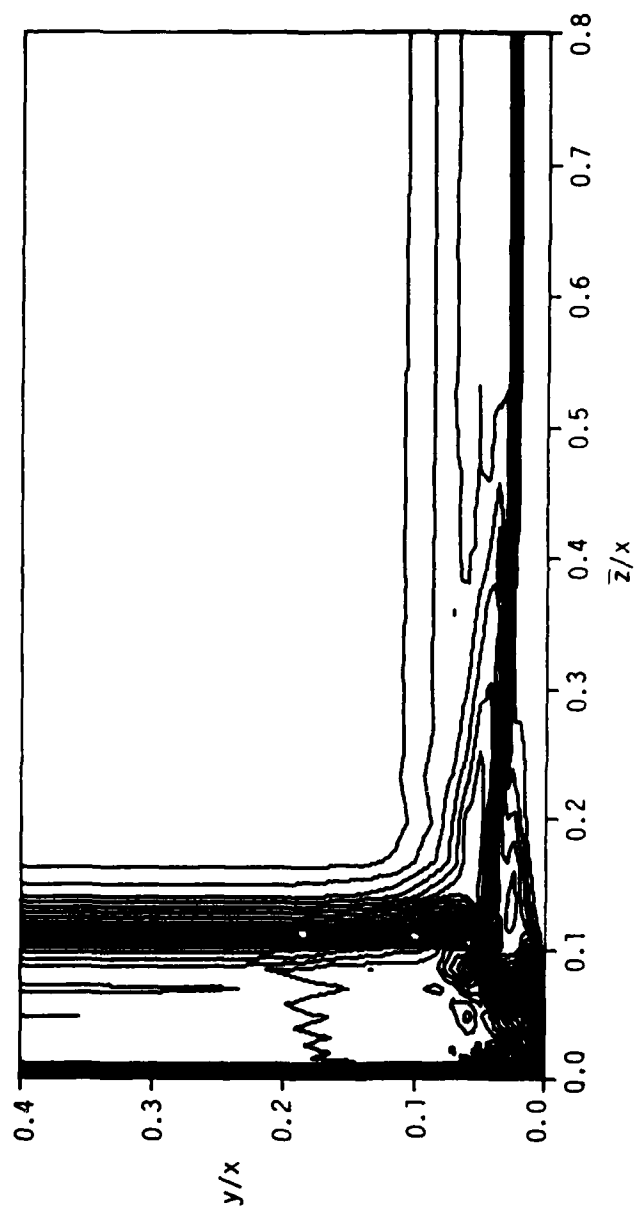


Figure 17. Density Contours

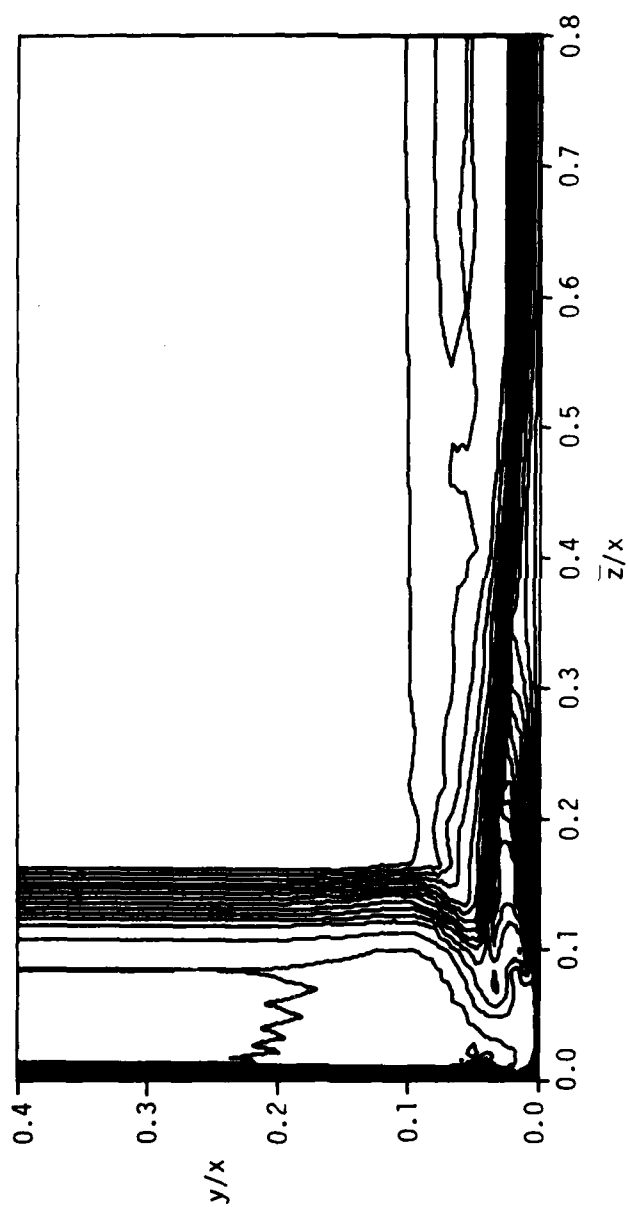


Figure 18. Mach Number Contours

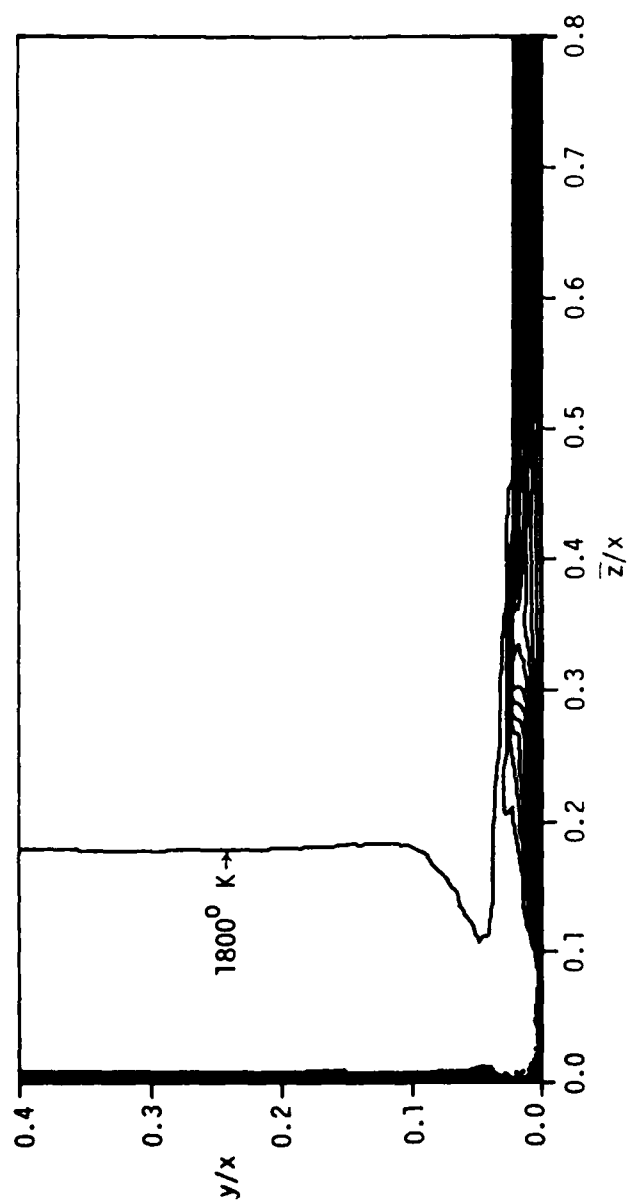


Figure 19. Total Temperature Contours

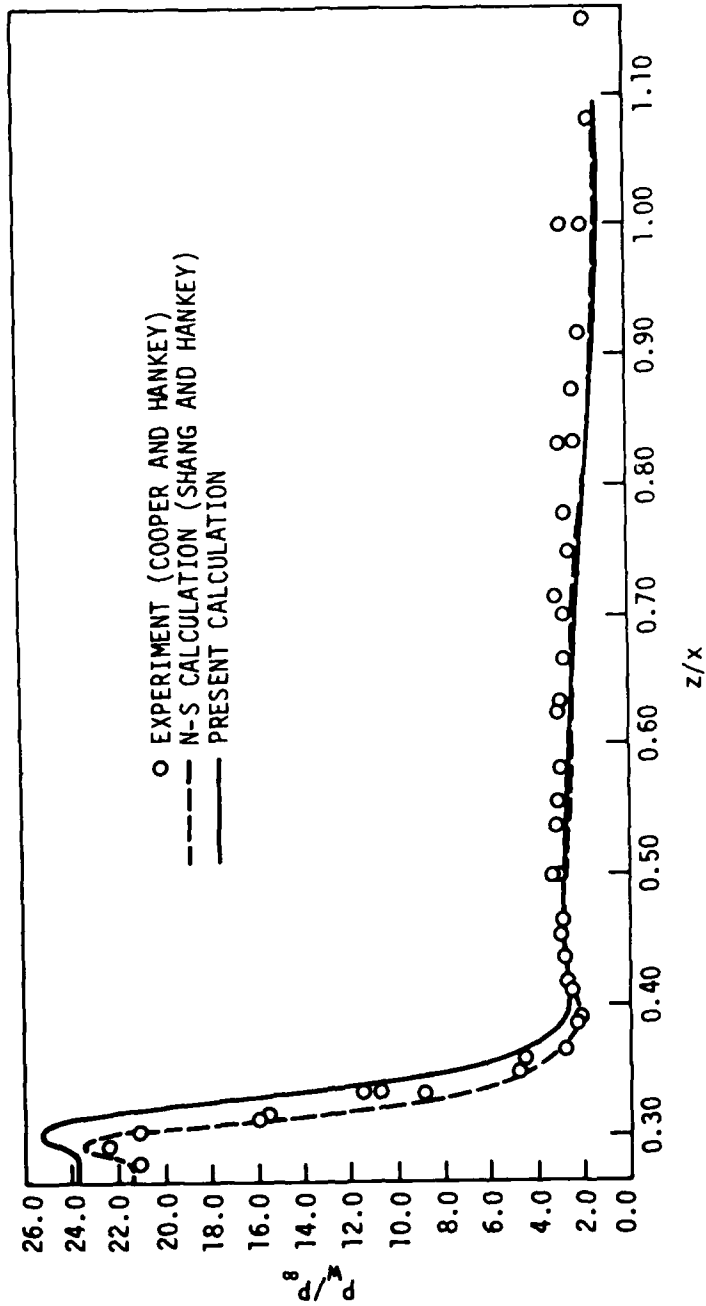


Figure 20. Comparison of Wall Pressure

not in good agreement with the Navier-Stokes results. The computed peak heat transfer rate is only 24% of the peak heat transfer rate computed in Ref. 8. The present calculation required about 18 minutes of computer time on a CDC 7600 computer.

SECTION V

CONCLUSIONS

In this study, numerical solutions have been obtained for the three-dimensional, supersonic viscous flow in an internal corner. These solutions were computed by solving the unsteady Navier-Stokes equations subject to a local conical assumption. This assumption permits a solution to be obtained at a fraction of the cost required for a complete Navier-Stokes calculation because a given problem is reduced from four dimensions (3 space, 1 time) to three dimensions (2 space, 1 time).

The present method was used to compute a compression corner flowfield corresponding to the laminar experiment of West and Korkegi. Both a shock fitting and a shock capturing solution were obtained. The computed locations of the shock waves and slip surfaces were in excellent agreement with the experiment. As expected, the shock fitting approach gave a much "sharper" resolution of the flowfield. The two computed wall pressure distributions agreed reasonably well with each other and with the experimental distribution. The present results were in much better agreement with the full Navier-Stokes solution than previous results computed using the assumption of inviscid conical flow.

The present method was also used to compute an unsymmetrical corner flowfield corresponding to the laminar experiment of Cooper and Hankey. This particular corner configuration is not truly conical and for this reason, the present results agreed only qualitatively with the experimental results. However, it would appear that if an appropriate

Reynolds number were chosen that gave the correct boundary layer thickness, the present method would yield good results.

REFERENCES

1. Charwat, A. F. and Redekopp, L. G., "Supersonic Interference Flow Along the Corner of Intersecting Wedges," AIAA Journal, Vol. 5, March 1967, pp. 480-488.
2. West, J. E. and Korkegi, R. H., "Supersonic Interaction in the Corner of Intersecting Wedges and High Reynolds Numbers," AIAA Journal, Vol. 10, May 1972, pp. 652-656.
3. Kutler, P., "Numerical Solution for the Inviscid Supersonic Flow in the Corner Formed by Two Intersecting Wedges," AIAA Paper 73-675, Palm Springs, Calif., June 1973.
4. Shankar, V., Anderson, D., and Kutler, P., "Numerical Solutions for Supersonic Corner Flow," Journal of Computational Physics, Vol. 17, July 1975, pp. 160-180.
5. Marconi, F., "Internal Corner Flow Fields," AIAA Paper 79-0014, New Orleans, LA., Jan. 1979.
6. Cresei, R. J., Rubin, S. G., Nardo, C. T., and Lin, T. C., "Hypersonic Interaction Along a Rectangular Corner," AIAA Journal, Vol. 7, Dec. 1969, pp. 2241-2246.
7. Rubin, S. G. and Lin, T. C., "A Numerical Method for Three-Dimensional Viscous Flow: Application to the Hypersonic Leading Edge," Journal of Computational Physics, Vol. 9, 1972, pp. 339-364.
8. Shang, J. S. and Hankey, W. L., "Numerical Solution of the Navier-Stokes Equations for a Three-Dimensional Corner," AIAA Journal, Vol. 15, Nov. 1977, pp. 1575-1582.
9. Hung, C. M. and MacCormack, R. W., "Numerical Solution of Supersonic Laminar Flow Over a Three-Dimensional Compression Corner," AIAA Paper 77-694, Albuquerque, N. Mex., June 1977.
10. Hung, C. M. and MacCormack, R. W., "Numerical Solution of Three-Dimensional Shock Wave and Turbulent Boundary Layer Interaction," AIAA Paper 78-161, Huntsville, Ala., Jan. 1978.
11. Shang, J. S., Hankey, W. L., and Petty, J. S., "Three-Dimensional Supersonic Interacting Turbulent Flow along a Corner," AIAA Journal, Vol. 17, July 1979.

12. Anderson, D. A., Private communication to W. L. Hankey, Aug. 1973.
13. McRae, D. S., "A Numerical Study of Supersonic Cone Flow at High Angle of Attack," AIAA 76-97, Washington, D.C., January 1976.
14. Vigneron, Y. C., Rakich, J. V., and Tannehill, J. C., "Calculation of Supersonic Viscous Flow over Delta Wings with Sharp Subsonic Leading Edges," AIAA Paper 78-1137, Seattle, Wash., July 1978.
15. Bluford, G. S., "Navier-Stokes Solution of Supersonic and Hypersonic Flow Field Around Delta Wings," AIAA Paper 78-1136, Seattle, Wash., July 1978.
16. McRae, D. S. and Hussaini, M. Y., "Numerical Simulation of Supersonic Cone Flow at High Angle of Attack," ICASE Report No. 78-21, Nov. 1978.
17. MacCormack, R. W. and Baldwin, B. S., "A Numerical Method for Solving the Navier-Stokes Equations with Applications to Shock-Boundary Layer Interactions," AIAA Paper 75-1, Pasadena, California, January 1975.
18. Tannehill, J. C., Holst, T. L., and Rakich, J. V., "Numerical Computation of Two-Dimensional Viscous Blunt Body Flows with an Impinging Shock," AIAA Journal, Vol. 14, February 1976, pp. 204-211.
19. Tannehill, J. C., Holst, T. L., and Rakich, J. V., "Numerical Computation of Two-Dimensional Viscous Blunt Body Flows with an Impinging Shock," AIAA Paper 75-154, Pasadena, California, Jan. 1975.
20. Cooper, J. R. and Hankey, W. L., "Flowfield Measurements in an Asymmetric Axial Corner at $M = 12.5$," AIAA Journal, Vol. 12, October 1974, pp. 1353-1357.

END

DATE
FILMED

8-80

DTIC